

Influence of solar tracking error on the performance of a small-scale linear Fresnel reflector



A. Barbón^a, C. Bayón-Cueli^c, L. Bayón^{b,*}, P. Fortuny Ayuso^b

^a Department of Electrical Engineering, University of Oviedo, Spain

^b Department of Mathematics, University of Oviedo, Spain

^c Polytechnic School of Engineering of Gijón, University of Oviedo, Spain

ARTICLE INFO

Article history:

Received 29 April 2020

Received in revised form

24 July 2020

Accepted 27 July 2020

Available online 11 August 2020

Keywords:

Small-scale linear fresnel reflector

Solar tracking system

Solar tracking error

ABSTRACT

Solar tracking systems are an indispensable requirement for optimal efficiency in small-scale linear Fresnel reflector systems. A thorough study of the influence of solar tracking errors on energy production is, therefore, required. The power produced by each mirror at any moment is also explicitly computed, as well as its variation under error. We study the large effect that the distance between the mirror and the absorber tube, solar time, and the day of the year have on the variation of power. Our results provide the foundations for the analysis of small-scale solar tracking systems. Solar tracking errors of less than 0.09° are acceptable (they cause power losses less than 1%), whereas errors larger than 0.36° start being noticeable (power losses greater than 3%).

© 2020 Elsevier Ltd. All rights reserved.

1. Introduction

The current status of energy production and the corresponding international policies require the development of new sustainable production systems. In 2019, the electricity generated from wind and solar energy in the EU was 402.8 TWh and 138.6 TWh, respectively [1]. The advantage of solar systems is that they can be deployed at small scale, allowing for their installation in many types of buildings, where they can be used for both thermal energy and electricity production. Notice that the household sector amounts to approximately 26% of total energy consumption in the EU [2], and that space heating and hot water accounted for 20.5% of the total final energy consumption in the EU in 2019 [3].

According to size, solar thermal systems can essentially be divided into one large-scale and small-scale ones. The former are considerably more complex and more expensive but also have higher efficiencies. They take the form of Central Solar Heating Plants (CSHP) with diurnal storage, which can be used to supply heat to district heating systems (residential building areas, hospitals, hostels or large buildings), for either domestic hot water systems or space heating systems, which are usually water-based. Normally, a district heating system consists of a CSHP, a heat

storage facility, a distribution network and heat transfer substations; centralized heat production provides great flexibility in terms of the fuel choice and the possibility of seasonal storage [4]. There exist several commercial CSHPs in Europe: Silkeborg [5] (110 MWth) in Denmark, Vojens [6] (50 MWth), also in Denmark, Crailsheim [7] (5.1 MWth) in Germany, for instance.

Small-scale systems are normally used in small-family houses, for domestic hot water systems and space heating.

A key element in any solar heating system is the solar collector, which can be either concentrating (parabolic trough [10], small-scale linear Fresnel reflectors (SSLFR) [11]) or non-concentrating (flat plane collectors [8] or evacuated tubes [9]). We focus on an SSLFR, in this paper. A comparison between parabolic trough collectors and SSLFRs can be read in Refs. [12]. The latter have some advantages over the former: lower structural requirements, lower maintenance, and lower cost but have the drawback of less efficiency. Some of the applications of SSLFRs in the building sector are shown in Ref. [13].

Due to their nature, the efficiency of an SSLFR depends on the accuracy of its optics and the absence of errors, so that a thorough analysis of these is required, which is the aim of this paper. Each component of the SSLFR (see Fig. 1) can be the source of optical errors. These can be partially overcome by increasing the efficiency of the primary reflector system and its tracking elements. There are also external parameters giving rise to potential errors [14], some of which can be grouped as follows:

* Corresponding author.

E-mail address: bayon@uniovi.es (L. Bayón).

Nomenclature			
A_{effi}	Effective area of the absorber tube (m^2)	W_{ai}^e	W_{ai} with tracking error (m)
CL_g	Cleanliness factor of the glass	α_b	Absorptivity of the absorber tube
CL_m	Cleanliness factor of the mirror	α_i	Angle between the vertical at the focal point and the line connecting it with the center point of each mirror ($^\circ$)
D	Diameter of the absorber tube (m)	α_i^e	α_i with tracking error ($^\circ$)
DNI	Direct Normal Irradiance (W/m^2)	α_S	Height angle of the Sun ($^\circ$)
d_i	Separation between $i - th$ and $i + 1 - th$ mirrors (m)	β_i	Tilt of $i - th$ mirror ($^\circ$)
f	Height of the receiver (m)	β_i^e	β_i with tracking error ($^\circ$)
IAM_i	Incidence angle modifier of $i - th$ mirror	δ	Declination of the sun ($^\circ$)
l_{abs}	Total illuminated length of the single absorber tube (m)	ϵ	Tracking error ($^\circ$)
l_{ciai}	Length of the circumference illuminated on the absorber by the $i - th$ mirror (m)	Γ	Day angle (h)
L_i	Position of $i - th$ mirror (m)	γ_S	Azimuth of the sun ($^\circ$)
L_M	Length of the mirrors (m)	η_{opt}	Optical efficiency (%)
n	Number of mirrors at each side of the central mirror	θ_i	Angle between the normal to the mirror and the incidence ray of the sun ($^\circ$)
n_d	Ordinal of the day	θ_i^e	θ_i with tracking error ($^\circ$)
Q	Total power absorbed (W)	θ_t	Transversal incidence angle ($^\circ$)
Q^e	Q with tracking error (W)	θ_z	Zenith angle of the Sun ($^\circ$)
T	Solar time (h)	ρ	Reflectivity of the primary mirrors
W_M	Width of the mirrors (m)	ρ_{cr}	Reflectivity of the receiver cavity
W_{ai}	Width illuminated on the absorber by the $i - th$ mirror (m)	τ	Transmissivity of the glass
		ω	Hour angle ($^\circ$)

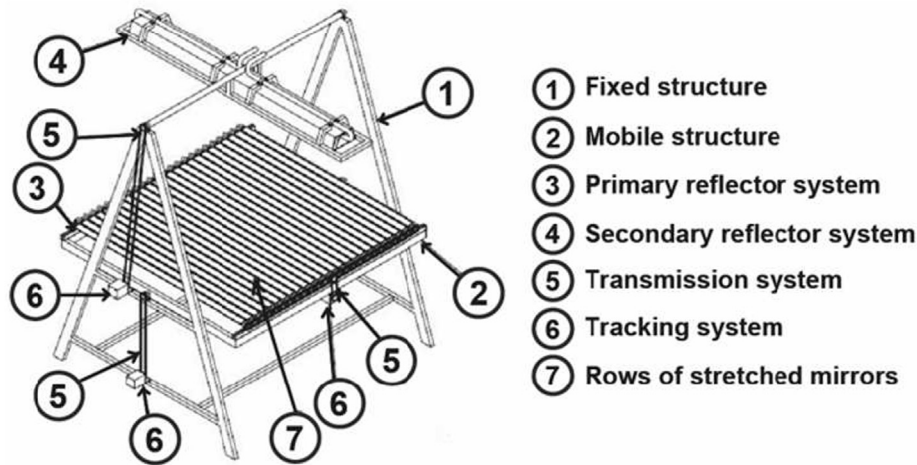


Fig. 1. SSLFR main blocks.

- (i) Estimations of the shape of the Sun [15,16]: these affect the focus width and, as a consequence, the size of the secondary reflector system.
- (ii) Physical properties of the materials [17], mainly specularity, reflectivity, roughness. The absorptivity of the absorber tube and the transmissivity of the glass cover contribute also to the loss of performance.
- (iii) Design issues, like the shape of the secondary reflector system. In recent years, this has been the topic of a number of studies, giving rise to many suggestions for its shape: compound parabolic [18], parabolic double tube [19], parabolic [20] and involute [20]. See Ref. [19,21] for studies on the relative efficiencies of the different options.
- (iv) Manufacturing errors, especially possible misalignments of: the main structure, the pivoting points of the mirrors, the

- secondary reflector system, the absorber tube or the transmission systems. The pivoting points of the mirrors have a significant effect on the solar tracking error if the eccentric distances are more than several centimeters: Zheng et al. [22] study the case of an eccentric distance of 5 cm on the Winter solstice at 8:00, getting a solar tracking error of 0.18° . (Notice that they do not study the energy loss).
- (v) Installation conditions, especially the lack of proper North-South orientation of the SSLFR [22]. The tracking algorithms are assume a geographic North-South orientation, but in the installation of solar collectors, the geomagnetic North-South orientation is used. Zheng et al. [22] study the solar tracking error for different deviations from the optimum North-South orientation, specifically on the Winter solstice

at 8:00, 12:00 and 18:00, for a 10° -East deviation. As in the previous case, they do not study the power losses.

- (vi) Operating conditions: tracking system, cleanliness of the mirrors and the glass cover, wind load, stress ...

These errors are evaluated independently [15,22], and their can be gathered to form an overall optical error [15].

As the SSLFR under study concentrates only the direct solar irradiance, the tracking system is needed to adjust the orientation of the mirrors according to the position of the Sun, which can be calculated using astronomical formulas [23–26]. In the absence of error, those formulas would be enough. However, manufacturing issues and installation and operating conditions of the SSLFR influence the precise orientation of each mirror, possibly giving rise to solar tracking errors decreasing the performance of the system. As is widely known, the solar tracking error affects SSLFRs significantly [15], the study of this influence is the main aim of this paper.

We call the attention of the reader to Ref. [27], where the authors carry out a similar study. The main differences with our work are: they discard both blocking and shadowing (whereas we design our system in order to avoid them); they do not consider a secondary reflector system (which we do); and they use statistical optics techniques (distributions and point spread functions) whereas we compute the value Q^e of power produced under solar tracking error by means of geometric and analytic arguments.

As regards tracking algorithms, Table 1 shows some of the most common ones, together with their theoretical accuracy. Despite their goodness, the tracking system is always subject to unpredictable manufacturing, software and maintenance issues. Hence, a thorough assessment of the effect of solar tracking errors on the performance of the system is required. This is the main topic of our work.

Zheng et al. [22] study the solar tracking error caused by other deviations such as the pivoting points of the mirrors, North-South orientation deviation, etc. but their results are presented as angular errors, not power losses. As such, their relevance with respect to the loss of energy associated to the source of optical error is very difficult to assess. We present our results as loss (percentage) of energy as a function of the solar tracking error, thus providing a clearer explanation, in our view.

We provide an analytical study of the influence of the solar tracking error on two values: the transversal length of the absorber tube effectively illuminated by the system and the effective power/energy reaching the absorber tube. Note that two different studies are possible: transversal and longitudinal. We only cover the first one, which is where the influence of solar tracking errors is noticeable. This part of our study covers the rays reaching the absorber tube directly. We take advantage of the Principle of Conservation of Energy in order to accurately compute the generated power. In the subsequent section, also using Conservation of Energy, we are able to carry out an analysis of the power produced by the rays reaching the secondary reflector.

The specific contributions of this paper can be summarized as follows:

- (i) A mathematical model is proposed to calculate the effective transversal length of the absorber tube illuminated by the primary reflector system (see Fig. 1), as well as the power it receives.
- (ii) Another model is proposed to compute the length of the absorber tube which is illuminated, and the variation of power absorbed by the tube under solar tracking errors.
- (iii) A detailed analysis estimating the influence of the solar tracking error on the power absorbed by the absorber tube coming from each mirror, depending on the day of the year and the solar time.

We present two novel analytic studies together we several numerical simulations which we have not encountered in the existing literature. First, we carry out a thorough study of the influence of the cosine of the incidence angle; a detailed analysis of the effective area illuminated on the absorber tube, together with the Principle of Conservation of Energy allows us to find a simple way to compute the absorbed power under the existence of a secondary reflector system, either with or without solar tracking error. Secondly, we give closed formulas for computing the illuminated length on the absorber tube under solar tracking errors.

Those analysis allow us to also find the optimal discretization for the tracking system (see Fig. 1): how often and by how much must the mirrors be moved in order to obtain the optimal performance?

The paper is organized as follows. In Section 2, some constructive aspects of an SSLFR are presented. The movement of the mirrors of the SSLFR is described in Section 3, together with the main formulas to be used later on. Section 4 covers the fundamental role of the Principle of Conservation of Energy in our study and its use in order to compute the power absorbed by the system in optimal conditions. In Section 5 we study the influence of solar tracking errors on power generation and Section 6 includes the results and discussion of our analysis. Finally, Section 7 covers our conclusions and some suggestions for future research.

2. Some constructive aspects of an SSLFR

An SSLFR consists of a set of flat mirrors concentrating the direct solar irradiance onto a focal element with much smaller surface. This focal element is, in our case, an absorber tube containing some thermal fluid (capable of keeping its liquid state at high temperatures) which flows through a set of pipes. The system under study, of which a prototype has already been built, is shown in Fig. 1. In this study, the systems the of SSLFR that interest us are: the primary reflector system (3), and the secondary reflector system (4). The primary reflector system (3) consists of a row of parallel stretched mirrors (7), mounted on an especially designed frame. Each mirror is pasted onto the frame using an industrial adhesive. They can be rotated on the north-south axis, so as to follow the sun's daily movement. The secondary reflector system (4) comprises the following elements: absorber tube, receiver cavity, isolation, glass covering, secondary structure, protective casing, and a secondary shaft. The absorber tube is especially coated so as to increase the absorption of the incident solar radiation and is encased in the receiver cavity to reduce convective heat losses. Moreover, the receiver cavity is sealed with a glass cover and silicon rubber beading. Others systems of the SSLFR are the following: fixed structure (1), mobile structure (2), transmission systems (5) and tracking system (6). See Refs. [29] for a more detailed description.

In order to precisely specify the setting, we shall assume the following conditions on the SSLFR (see Fig. 1):

- (i) It is perfectly aligned in the North-South direction.
- (ii) The mobile structure is perfectly horizontal.

Table 1
Accuracy of some Sun tracking algorithms.

Algorithm	Maximum error ($^\circ$)
Int. Solar Position Algorithm (SPA) [23]	0.0003
Grena Algorithm [28]	0.0027 – 0.01 – 0.04 – 0.2
Grena Algorithm [26]	0.0027
Blanco et al. [25]	0.008
Michalsky et al. [24]	0.01

- (iii) Each mirror in the primary reflector system pivots around its center. The mirrors are flat and reflective and have all the same length and width. Their flatness guarantees that the shape of the Sun does not affect the irradiance reaching the receiver cavity [30].
- (iv) The secondary reflector system is horizontal.
- (v) There is a single absorber tube.
 - On the contrary, we allow for errors in the following elements:
 - (i) The transmission system.
 - (ii) The tracking system.

3. Basic formulas of the SSLFR

Our SSLFR consists of $2n + 1$ mirrors, numbered from right to left, starting at 1; the center point of mirror $n + 1$ is in the midpoint of the SSLFR. The SSLFR is symmetrical with respect to the vertical axis joining the center of the absorber tube and the center of mirror $n + 1$. It is designed such that its performance is also symmetrical throughout the day.

The distances $d_i > 0$ between mirrors i and $i + 1$, and L_i between their centers, has been computed using the method in Ref. [16] for optimal shape: this method is based on assuming a “worst solar time” $\theta_t = \theta_{t_0}$ (roughly speaking, the angle at which the system is designed to start to generate power), and a “worst mirror”, which is the one farthest from the Sun at that solar time; this gives the minimum distance guaranteeing neither shading nor blocking between consecutive mirrors during the effectively productive time. The Technical Report [31] of the Spanish Government requires that, in order to minimize shadowing effects, the distance between mirrors has to guarantee at least 4 h of sunshine around noon on the Winter solstice. We have verified, as shown in Section 5, that using $\theta_{t_0} = 50^\circ$ for the locality under study (Almeria, Spain), that requirement is satisfied. Therefore, as during the operating hours of the SSLFR under study there is essentially neither shading nor blocking, we shall not consider them in this duty.

Usually, in order to simplify the manufacturing of the SSLFR, all the mirrors are equally separated by a common distance d .

The angle α_i between the vertical axis and the line joining the center of mirror i with the center of the absorber tube is (see Fig. 2(a)):

$$\alpha_i = \arctan \left[\frac{L_i}{f + D/2} \right]; \quad 1 \leq i \leq 2n + 1 \tag{1}$$

and is, by convention, always positive.

We remark that, in the SSLFR under study, all the mirrors move in synchrony, at the same angular speed (they are, in fact, joined to the rotary system controlling the central one).

The angle the Sun rays form with the vertical axis (solar angle θ_t) at time t of each day is given by Ref. [32]:

$$\theta_t = \arctan \left(\frac{\sin \gamma_S}{\tan \alpha_S} \right) \tag{2}$$

where α_S is the solar altitude and γ_S is the solar azimuth.

The tilt angle β_i of mirror i , defined as the angle the mirror forms with the horizontal plane, depends on θ_t and is defined in such a way that the Sun ray meeting the midpoint of that mirror must be reflected towards the center of the absorber tube. This gives:

$$\beta_i = \frac{-\theta_t \pm \alpha_i}{2}; \quad 1 \leq i \leq 2n + 1 \tag{3}$$

The sign \pm is chosen as: $-$ for the left side and $+$ for the right side of the SSLFR. We also consider, by convention, $\beta_i > 0$ when measured counter-clockwise above the horizontal axis. For the central mirror, we have:

$$\beta_{n+1} = \frac{\theta_t}{2} \tag{4}$$

4. The Principle of Conservation of Energy

The thermal energy produced by an SSLFR over a given period of time can be estimated from the solar irradiance reaching the absorber tube. Issues related to thermal properties of the system (out of the scope of this work) require the knowledge of the total illuminated length of the absorber tube (one can think, for instance, of the goodness of the transmission of heat to the thermal fluid). Before proceeding, we describe some specific features of the SSLFR under study.

The power absorbed by the absorber tube, Q , is, traditionally,

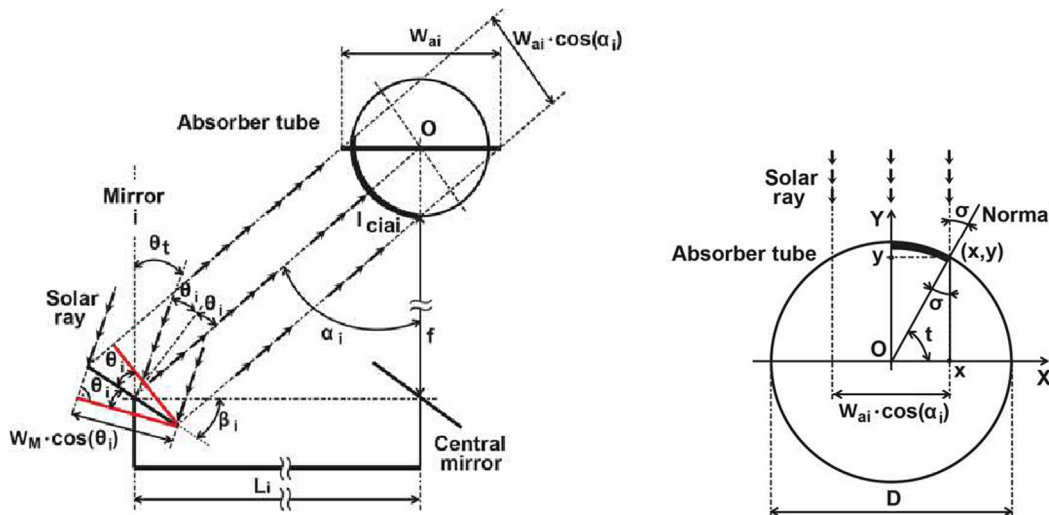


Fig. 2. Applying the principle of conservation of energy.

computed using some simplifications (see for example [33,34] or [35]), by means of the formula:

$$Q = DNI \cdot \eta_{opt0} \cdot IAM \cdot A_m \cdot x_{field} \cdot \eta_{endloss} \quad (5)$$

where DNI denotes the direct normal irradiance; and η_{opt0} stands for the optical efficiency of the SSLFR for normal incident rays (i.e. whose incidence angle equals zero). The value A_m is the total mirror area of the collector, x_{field} is the availability of the solar field, and $\eta_{endloss}$ is the end loss efficiency, which measures the area of the receiver which is not illuminated by the reflected rays. Finally, the Incidence Angle Modifier (IAM) (see Ref. [27,33,34,36–39]), is a catch-all coefficient which includes all the uncontrolled losses both in the optics of the concentrator and in the receiver: shadowing, blocking of reflected rays, incidence cosine for each mirror element, effective mirror aperture area ... Ray-tracing is used to assess the IAM , and is usually subdivided into its transversal and longitudinal components:

$$IAM = IAM_T(\theta_t) \cdot IAM_L(\theta_l) \quad (6)$$

When the longitudinal study is not carried out, the corresponding $\eta_{endloss}$ and IAM_L are given the value 1.

This model provides an approximation to Q which is often good enough, assuming (among other things) that all the solar rays reflected by the primary field reach the secondary system. However, as errors can (and will probably) happen, we need a much more precise model allowing us to properly evaluate the influence of solar tracking errors. Thus, following [38,40], we shall study the contribution of each mirror on the absorber tube and the quantity of light reaching this element from each of the mirrors in the primary reflector system.

We divide this study in two cases: the rays reaching the absorber tube directly from the mirrors, and those who are reflected by the secondary system.

4.1. Case I: solar rays directly incident on the absorber tube

We start by computing the transversal length l_{ciai} of the arc of circumference of the absorber tube illuminated by mirror i . For the rays which fall directly on the tube, we get:

$$l_{ciai} = \begin{cases} D \cdot \arcsin\left(\frac{W_{ai} \cdot \cos\alpha_i}{D}\right) & \text{if } W_{ai} \cdot \cos\alpha_i < D \\ \frac{\pi D}{2} & \text{if } W_{ai} \cdot \cos\alpha_i \geq D \end{cases} ; 1 \leq i \leq 2n + 1 \quad (7)$$

where W_{ai} is the width of the tube illuminated by the i -th mirror (m). Its value is computed in Ref. [41]:

$$W_{ai} = W_M \cdot [\cos\beta_i \pm \sin\beta_i \tan\alpha_i]; 1 \leq i \leq 2n + 1 \quad (8)$$

The sign \pm is taken according to the following criteria: $-$ for the left side, and $+$ for the right side of the SSLFR. Fig. 2 shows these parameters. In Fig. 2(a), θ_i is the angle between the normal to the mirror and the angle of incidence of the Sun, and O is the center of the location of the absorber tube. In addition, the point O is the center of W_{ai} .

In order to compute the power absorbed, we must study the cosine factor of the incidence angle each ray forms with the absorber tube. In Fig. 2(b), the variation of this cosine factor for each ray depending on the point of the arc of length l_{ciai} is shown (for the i -th mirror). Taking into account this effect at each point leads one

to compute the line integral:

$$\int_C \cos(\sigma) ds \quad (9)$$

where $\cos(\sigma)$ is a value depending on each point of C . As the arc of circumference C can be parametrised as:

$$\begin{cases} x(t) = \frac{D}{2} \cos t = \frac{D}{2} \sin \sigma \\ y(t) = \frac{D}{2} \sin t = \frac{D}{2} \cos \sigma \end{cases} ; 0 \leq \sigma \leq \sigma_i = \arcsin \frac{W_{ai} \cdot \cos \alpha_i}{D}$$

using $ds = \|(x'(t), y'(t))\| = \frac{D}{2}$ and applying the definition of line integral, we obtain:

$$\int_C \cos(\sigma) ds = 2 \int_0^{\sigma_i} \cos(\sigma) \frac{D}{2} d\sigma = D \sin \sigma_i = W_{ai} \cdot \cos \alpha_i \quad (10)$$

We shall call A_{effi} (m^2) (the effective area illuminated on the absorber tube by mirror i), the quantity:

$$FA_{effi} = l_{abs} \cdot \int_C \cos(\sigma) ds; 1 \leq i \leq 2n + 1 \quad (11)$$

where l_{abs} is the longitudinal length of the absorber tube which is illuminated. As we are only carrying out the transversal study, l_{abs} will be a fixed specific value. Then:

$$A_{effi} = l_{abs} \cdot W_{ai} \cdot \cos \alpha_i; 1 \leq i \leq 2n + 1 \quad (12)$$

Some elementary operations give:

$$W_{ai} \cdot \cos \alpha_i = W_M \cdot [\cos \beta_i \pm \sin \beta_i \tan \alpha_i] \cdot \cos \alpha_i \quad (13)$$

$$= W_M \cdot [\cos \beta_i \cos \alpha_i \pm \sin \beta_i \sin \alpha_i] = W_M \cos(\beta_i \mp \alpha_i) \quad (14)$$

But if θ_i is the angle formed by the normal to the i -th mirror and the incidence angle of the Sun, the following equality holds:

$$\cos \theta_i = \cos(\beta_i \pm \alpha_i)$$

with $+$ for the left side, and $-$ for the right side of the SSLFR, so that:

$$W_{ai} \cdot \cos \alpha_i = W_M \cdot \cos \theta_i \quad (15)$$

which, finally, gives:

$$A_{effi} = l_{abs} \cdot W_M \cdot \cos \theta_i; 1 \leq i \leq 2n + 1 \quad (16)$$

This important result is no more than a consequence of the Principle of Conservation of Energy (PCE): “the energy reflected by the primary mirror must equal the energy absorbed by the tube.”

Hence, assuming that all rays fall on the absorber tube, we propose the following formula for computing the power Q absorbed by the tube, which depends on the effective area of each mirror:

$$Q = \sum_{i=1}^{2 \cdot n + 1} DNI \cdot \eta_{opt} \cdot l_{abs} \cdot W_M \cdot \cos \theta_i \quad (17)$$

where:

- (i) The direct normal irradiance (DNI) (W/m^2) is obtained from a satellite database. We have used PVGIS [42] to obtain

monthly averages per day of its value. We transform these averages into a continuous distribution of beam solar irradiance by means of Fourier Series, as in Refs. [43].

- (ii) The total optical yield (η_{opt}) (dimensionless) is calculated considering the reflectivity of the mirrors (ρ), the cleanliness factors of the mirror (Cl_m) and of the glass covering of the secondary reflector system (Cl_g), the transmissivity of this glass (τ), and the absorptivity of the material of which the absorber tube is made (α_b):

$$\eta_{opt} = \rho \cdot Cl_m \cdot Cl_g \cdot \tau \cdot \alpha_b \tag{18}$$

Although some of the parameters contributing to η_{opt} , especially τ , vary with the angle of incidence (see Ref. [17]), we consider them constant for simplicity (see Ref. [27,44,45]).

- (iii) The parameters l_{abs} y W_M are fixed.
- (iv) The incidence angle θ_i of mirror i , (and, from it, its cosine $\cos\theta_i$) can be computed, for example, as:

$$\theta_i = \pm\theta_t \pm\beta_i; \quad 1 \leq i \leq 2n + 1 \tag{19}$$

where the sign \pm follows the criteria: $-$ for solar time $T \leq 12$, and $+$ for solar time $T > 12$.

Therefore, in perfect conditions, the power absorbed by the absorber tube can be assumed directly proportional to the length of the arc of circumference illuminated (l_{ciai}) on the absorber tube by the i -th mirror and the cosine of the incidence angle:

$$Q = \sum_{i=1}^{2 \cdot n + 1} K \cdot W_M \cdot \cos\theta_i \tag{20}$$

The proportionality constant K is the product of DNI , η_{opt} , and l_{abs} .

As we show in what follows, the PCE allows us to study the influence of the receiving cavity with great precision and, as a consequence, to properly analyze the effect of solar tracking errors.

4.2. Case II: solar rays falling indirectly on the absorber tube

We end this section with a remark on the receiver cavity which is usually (practically always) part of the secondary reflector system. As we have already explained, many different shapes have been proposed for it: compound parabolic, parabolic double wing, parabolic, involute, etc. This variety and the inherent complexity of each one forces one to make numerical simulations in order to assess the influence of solar tracking errors. By way of example and, because it is the one used in our prototype [13], we are going to study an involute-shaped receiver cavity.

The line normal to the involute of a circumference (in our case, the absorber tube) is tangent to the latter. However, the mere study of the rays reflected by the involute requires computing intersections of lines with the curve given by the following parametric equations:

$$\begin{cases} x(t) = r(\sin(t) - t \cos(t)) \\ y(t) = r(\cos(t) + t \sin(t)) \end{cases} \tag{21}$$

This requires solving transcendent equations, forcing one to use numerical approximations: there is no analytic solution to the problem of computing the arc-length of the absorber tube illuminated by the rays reflected on the involute. This is why ray-tracing programs are used for it. See, for instance Ref. [46], where a MATLAB program was used: with it we have obtained Fig. 3.

Obviously, in the absence of a receiver cavity, the maximum illuminated length can only be $\frac{\pi D}{2}$. This is what makes the choice of

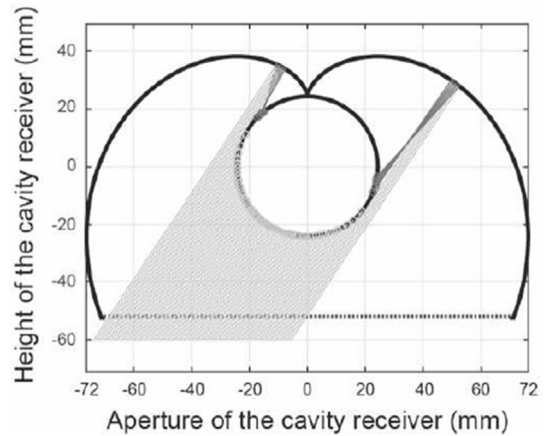


Fig. 3. Ray tracing simulation for a receiver cavity.

the diameter of the absorber tube an essential point. When $W_{ai} \cdot \cos\alpha_i > D$, there will be a quantity of rays which do not fall on the absorber tube (so to say, “lost” rays). The length of this family of lost rays is:

$$l_{cr} = W_{ai} \cdot \cos\alpha_i - D \tag{22}$$

But, by the PCE, it is not this length what matters in order to compute the absorbed power. Under the (reasonable) assumption that the rays not falling on the tube do fall into the receiver cavity, as the geometry of the involute implies that they will fall on the tube, and

$$W_{ai} \cdot \cos\alpha_i = W_M \cdot \cos\theta_i \tag{23}$$

we can then conclude that the power Q absorbed by the absorber tube, in an SSLFR with receiver cavity in the shape of an involute is:

$$Q = \begin{cases} \sum_{i=1}^{2 \cdot n + 1} K \cdot W_M \cdot \cos\theta_i & \text{if } W_{ai} \cdot \cos\alpha_i < D \\ \sum_{i=1}^{2 \cdot n + 1} K \cdot D & \text{if } W_{ai} \cdot \cos\alpha_i = D \\ \sum_{i=1}^{2 \cdot n + 1} K \cdot (D + l_{cr} \cdot \rho_{rc}) & \text{if } W_{ai} \cdot \cos\alpha_i > D \end{cases} \tag{24}$$

where the rays falling into the cavity are affected by its reflectivity: ρ_{rc} .

5. Analysis of the solar tracking error

Let us make some preliminary considerations on the dependence of some elements of Eq. (17) with respect to the solar tracking error:

- (i) The DNI is not affected by solar tracking errors.
- (ii) Concerning η_{opt} , although some of its constituent parameters (mainly τ) change with the angle of incidence (see Ref. [17]), we consider them constant for simplicity (see Ref. [44,45]).
- (iii) The parameter l_{abs} is constant, as we are only performing the transversal study.
- (iv) We do not need to consider shadowing or blocking because our design has already covered this issues.

As in the previous section, we divide this study into two parts:

the rays which fall directly on the tube and those reflected by the secondary system.

5.1. Part I: solar rays directly incident on the absorber tube

In this case, the impact of the solar tracking error on the power absorbed by the absorber tube is estimated using equation (20).

In order to simplify the exposition, we shall only consider a solar tracking error $\varepsilon > 0$ (in radians) such that:

$$\beta_i^e = \beta_i - \varepsilon; \quad 1 \leq i \leq 2n + 1 \quad (25)$$

As the mirrors have all the same angular velocity, all incur the same error. The length of the absorber tube illuminated by mirror i under solar tracking error ε is now:

$$W_{ai}^e = W_M \cdot [\cos \beta_i^e \pm \sin \beta_i^e \cdot \tan \alpha_i^e]; \quad 1 \leq i \leq 2n + 1 \quad (26)$$

where β_i^e ($^\circ$) is the tilt angle of i -th mirror under solar tracking error, and α_i^e ($^\circ$) is the angle (under solar tracking error) between the vertical at the theoretical focal point O and the line joining the midpoint mirror i with the true focal point (see Fig. 4). As above, the $-$ sign is used on the left side and $+$ on the right side of the SSLFR.

As Fig. 4 shows, the focal point under solar tracking error O' is the point of incidence of the solar rays coming from the center of mirror i , and consequently the midpoint of the segment W_{ai}^e . This is the most important effect of solar tracking error: the displacement of the geometric focal point O to O' . This (in general) causes a decrease in the total power absorbed by the absorber tube. If the solar tracking error is large, some of the reflected rays may even fall out of the secondary reflector system.

From the geometric elements in Fig. 4, we can deduce the value of α_i^e :

$$\alpha_i^e = \alpha_i \pm 2 \cdot \varepsilon; \quad 1 \leq i \leq 2n + 1 \quad (27)$$

where the sign \pm becomes $+$ on the left side, and $-$ on the right side. This allows us to compute the length $\overline{OO'}$:

$$\overline{OO'} = \pm(f + D/2) [\tan \alpha_i^e - \tan \alpha_i] \quad (28)$$

with the same sign criteria. Also:

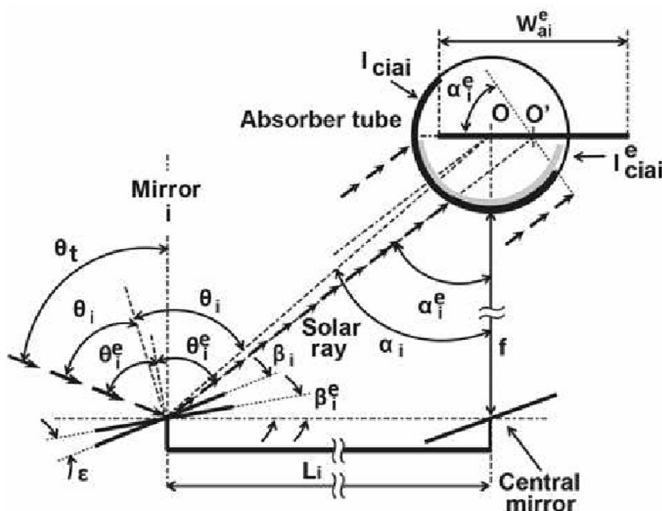


Fig. 4. Illustration of the effect of the solar tracking error.

$$\theta_i^e = \theta_i \pm \varepsilon; \quad 1 \leq i \leq 2n + 1 \quad (29)$$

where the sign \pm becomes now: $+$ for solar time $T \leq 12$, and $-$ for solar time $T > 12$.

Let us compute the length l_{ciai}^e of the circumference of the absorber tube illuminated by the i -th mirror under solar tracking error. Unlike in the theoretical case, in which the value can be deduced by geometric arguments, we now need to calculate the length of a curve $y(x)$ using the classical formula:

$$L = \int_a^b \sqrt{1 + y'^2(x)} dx \quad (30)$$

Centering the reference frame at O and rotating it so that the incident ray is parallel to the OY axis (see Fig. 5), the equation of the circumference of the tube is:

$$y(x) = \sqrt{(D/2)^2 - x^2} \quad (31)$$

whence, for each mirror i ($1 \leq i \leq 2n + 1$), the corresponding length will be:

$$l_{ciai}^e = \int_{a_i}^{b_i} \frac{D/2}{\sqrt{(D/2)^2 - x^2}} dx = D / 2 \arcsin \left[\frac{x}{D/2} \right]_{a_i}^{b_i}; \quad 1 \leq i \leq 2n + 1 \quad (32)$$

Notice that from our conventions, the endpoints of the segment $[r_i, l_i]$ corresponding to mirror i fall on the diameter with center O , perpendicular to the incident rays (under solar tracking error), when this diameter has been rotated α_i^e degrees with respect to the horizontal of the SSLFR. These endpoints can be computed explicitly:

$$[r_i, l_i] = [-(W_{ai}^e/2 + \overline{OO'}) \cdot \cos \alpha_i^e, (W_{ai}^e/2 - \overline{OO'}) \cdot \cos \alpha_i^e]; \quad 1 \leq i \leq 2n + 1 \quad (33)$$

The value l_i corresponds to the light ray reflected at the left endpoint of mirror i , and it can be either positive or negative, depending on ε . Equivalently, r_i corresponds to the right endpoint of mirror i and is always negative in our case (an error $\varepsilon > 0$ which decreases β_i). Thus, after computing the respective integrals, we only have to calculate the intersection of two intervals:

$$[a_i, b_i] = [r_i, l_i] \cap [-D/2, D/2]; \quad 1 \leq i \leq 2n + 1 \quad (34)$$

We can now assess the power Q^e absorbed by the absorber tube under solar tracking error, corresponding to the rays falling directly on it, by applying the PCE:

$$Q^e = \sum_{i=1}^{2 \cdot n + 1} K \cdot W_M \cdot \cos \theta_i^e \quad (35)$$

where K is the parameter introduced in Eq. (20). Notice how the only difference with (20) is the incidence angle θ_i^e .

5.2. Part II: solar rays reflected on the secondary system

As in the previous section, the only way to assess the influence of the solar tracking error on the length of the absorber tube illuminated by the rays reflected on the secondary reflector system is by means of ray-tracing simulations. However, using the PCE, it is quite elementary to compute the absorbed power Q^e . Assuming

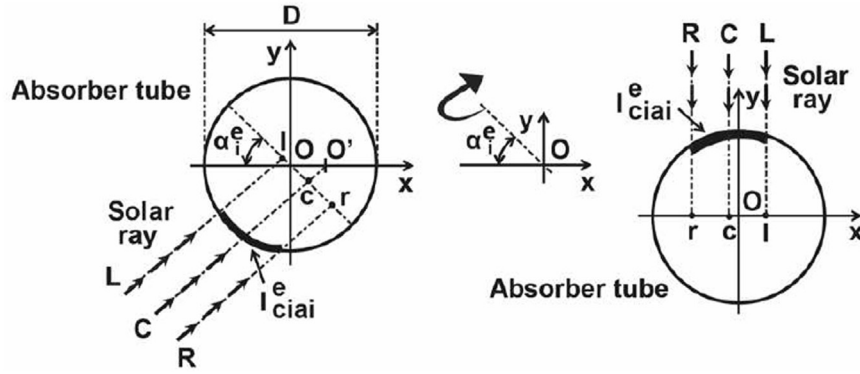


Fig. 5. Schematics for computing l_{crai}^e .

that the cavity is properly designed so that the displacement OO' does not cause any reflected rays to get out of it, then all the reflected rays will end up falling on the tube.

As above, a simple argument allows one to compute the length of the ray-field which does not fall directly on the tube, as the symmetric difference of two intervals: $[r_i, l_i]$ y $[a_i, b_i]$:

$$l_{cr}^e = (l_i - r_i) - (b_i - a_i); \quad 1 \leq i \leq 2n + 1 \quad (36)$$

so that, under the assumption that no rays go out of the reflecting cavity, we obtain:

$$Q^e = \begin{cases} \sum_{i=1}^{2 \cdot n+1} K \cdot W_M \cdot \cos \theta_i^e = \sum_{i=1}^{2 \cdot n+1} K \cdot (b_i - a_i) & \text{if } [r_i, l_i] \in [-D/2, D/2] \\ \sum_{i=1}^{2 \cdot n+1} K \cdot [(b_i - a_i) + l_{cr}^e \cdot \rho_{rc}] & \text{if } [r_i, l_i] \notin [-D/2, D/2] \end{cases} \quad (37)$$

6. Results and discussion

In this section we carry out the following analysis: (i) we study how the solar tracking error affects the power absorbed by the absorber tube; (ii) we evaluate the influence of that solar tracking error depending on the mirror, the day of the year, and the solar time. The SSLFR we consider in this section is the one proposed in Ref. [13], with the parameters listed in Table 2, and the geographic location of Almeria, Spain, which has a latitude of $36^\circ 50'07''N$,

Table 2
Parameters of the SSLFR in Section 6.

Parameters	Value
n	Number of mirrors at each side of the central mirror 12
W_M	Mirror width 0.06 (m)
D	Diameter of the absorber tube 0.0486 (m)
f	Height of the receiver 1.50 (m)
L_M	Mirror length 2.00 (m)
ρ	Reflectivity of the mirrors 0.94 [17]
ρ_{cr}	Reflectivity of the receiver cavity 0.9 [47]
CL_m	Cleanliness factors of the mirror 0.96 [48]
CL_g	Cleanliness factors of the glass in the secondary absorber 0.96 [48]
τ	Transmissivity of glass $\tau = 0.87$ if $\alpha_i \leq 20^\circ$, $\tau = 0.85$ if $20^\circ \leq \alpha_i \leq 30^\circ$ [49]
α_b	Absorptivity of the tube 0.95 [47]

longitude of $02^\circ 24'08''W$ and altitude of 22 m.

Recall that we only carry out the transversal study, so that the angle between the axis of each mirror and the horizontal plane is 0° , as is the angle between the absorber tube and the horizontal plane. We also assume that the illuminated length of the tube is equal to the mirror length $l_{abs} = 2.00$ (m). We have $d_{max} = 3.2$ (cm) and $d_{min} = 2.5$ (cm) as maximum and minimum distance between mirrors, for a total width of the SSLFR of 2.14 (m). All the parameters in Table 2 are constant. Finally, we assume that all light rays are parallel, disregarding the Sun's shape [50].

All our computations have been carried out using Mathematica™ code; we have developed modules for calculating: (i) the optimal design of the SSLFR in order to prevent blocking and shadowing; (ii) the direct normal irradiance, using data from the PVGIS [42] database and incorporating the meteorological conditions of the location [43]; (iii) the length of the circumference illuminated on the absorber tube by each mirror; (iv) the power absorbed by the SSLFR with and without secondary reflecting cavity; (v) the influence of the solar tracking error.

For instance, Fig. 6 shows the energy absorbed by the absorber tube in the Summer solstice (June 21st) coming from each mirror, assuming correct tracking, for Sun time T between 9 and 15 (an interval in which our SSLFR is designed to perform). Each column represents the absorbed energy coming from each mirror (indicated in the top row).

In Fig. 6, the total daily energy has been computed using a discretization of 1 min: we assume the Sun is motionless during each minute, which is obviously false. As a matter of fact, on that specific day, the Sun moves along all the 100° degrees $[-\theta_{t0}, \theta_{t0}]$ of the

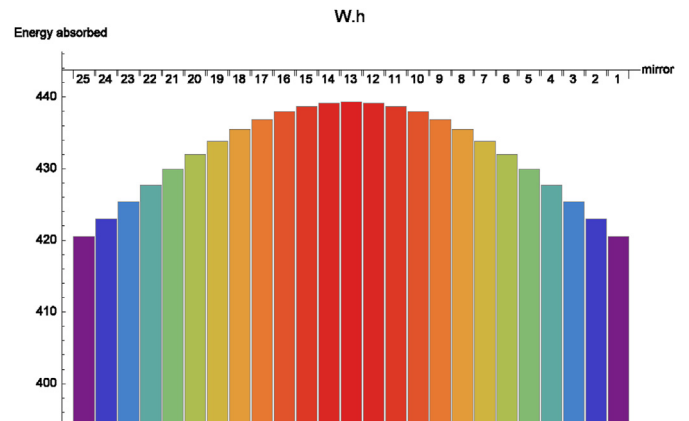


Fig. 6. Energy absorbed (June 21st) by SSLFR due to each mirror.

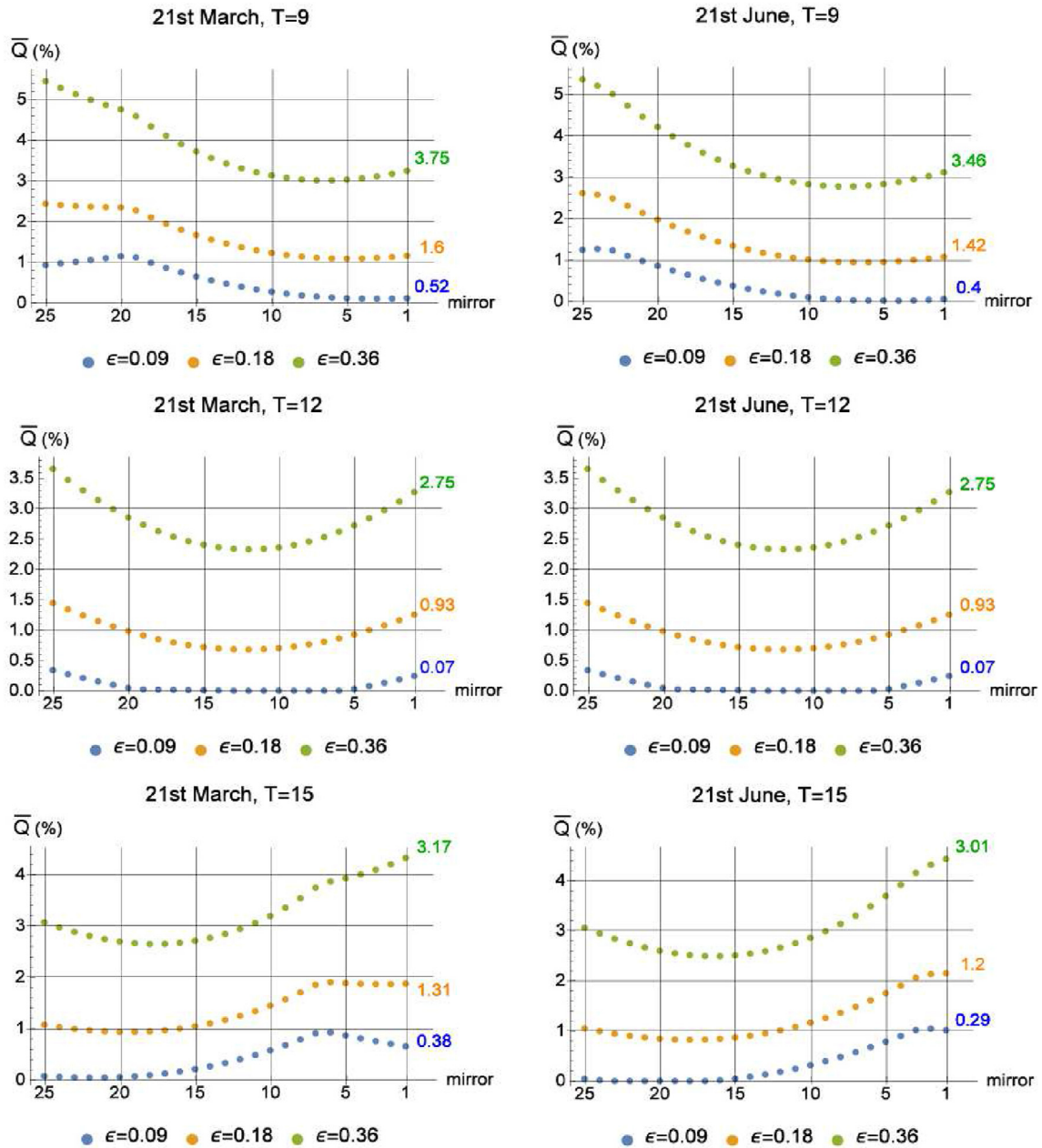


Fig. 7. Effects of the solar tracking error in the mirrors. (a) Spring equinox (21st March). (b) Summer solstice (21st June).

design, from 8 : 13 to 15 : 46 (solar time), which gives an approximate angular velocity of 0.22° per minute (although this velocity is not constant). Even more, this velocity depends (largely) on the day of the year (the Summer solstice is the slowest). In the Winter solstice (December 21st), the angular velocity of the Sun is about 0.41° per minute. As we explained in the Introduction, our analysis on the solar tracking error will allow us to decide whether that 1 min discretization is good enough or not.

We now provide the results of our analysis with different solar tracking errors: 0.09° , 0.18° and 0.36° , for each of the 25 mirrors composing the primary reflector system. We need to work with the instantaneous power, and we shall compute the difference between the power absorbed under solar tracking error (Q^e) and in the ideal case (Q). We provide results for different values of the day of the year, solar time and mirror. Specifically, for the Spring and Autumn

equinoxes (21st March and 21st September) and the Summer and Winter solstices (21st June and 21st December), at three different solar times: 9:00, 12:00 and 15:00. The data are summarized in Figs. 7 and 8. The values are % of power loss, with respect to the ideal case, that is:

$$\bar{Q} = \frac{Q - Q^e}{Q} \times 100 \quad (38)$$

On the right side of each plot, the relative mean loss is shown, for each solar tracking error ϵ : apart from its intrinsic interest, it shows how the loss due to the extremal mirrors is less important than it seems (they contribute less to the total absorbed power, so that losses in them have less impact).

We wish to remark the following:

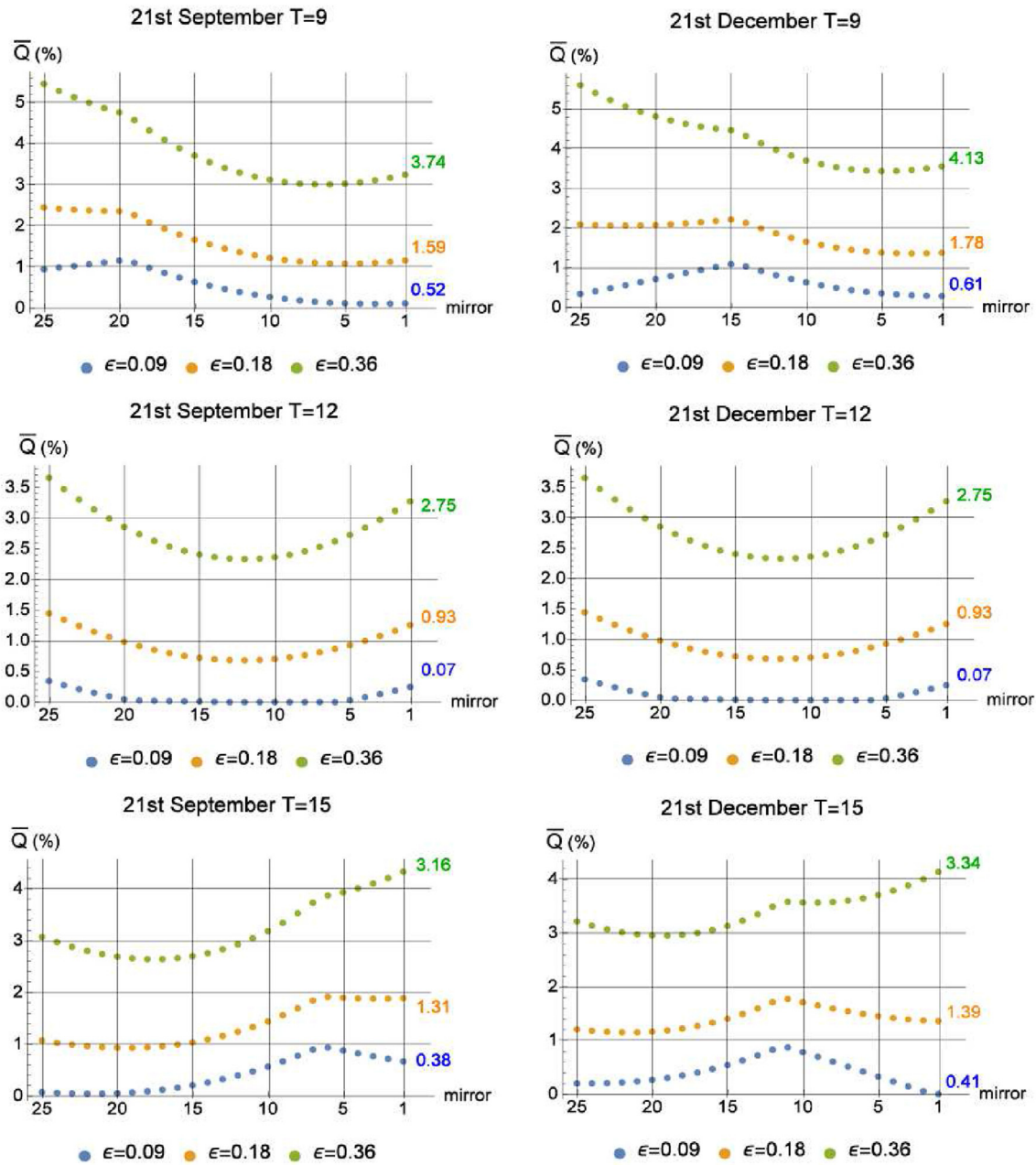


Fig. 8. Effects of the solar tracking error in the mirrors. (a) Autumn equinox (September 21st). (b) Winter solstice (December 21st).



Fig. 9. Error without cavity receptor.

1. The loss pattern is exactly the same at noon, on each of the four days. Actually, this happens regardless of the day of the year, as a consequence of our transversal-only study.
2. There is a high non-linearity in the influence of solar tracking error on power loss.
3. The plots are not symmetrical: this is because we are assuming the same error on all the mirrors (they all increase their inclination by ϵ).
4. The maximum power loss does not necessarily happen for one of the extremal mirrors (this is especially clear on the 21st March and the 21st September at 9:00 and 15:00).
5. Despite looking so, the plots at 9:00 and 15:00 are not mirror-images of each other. They have similar shapes (reflected on the central axis) but, because the errors are all in the same direction throughout the day, they have more influence in the

morning than in the evening. However, if instead of adding ε , we subtracted it, we would then get the corresponding symmetric plots.

- Finally, a solar tracking error of 0.09° has a maximum loss of power of 0.61%, which, when considered in a real-world setting would probably become negligible compared to other issues (dirt, pollution, cloudiness ...).

At this point, we can confirm that Fig. 6 is accurate enough: recall that, to produce it, we assumed that the Sun's position was constant during each minute. In that minute, θ_t varies approx. 0.22° , and as we know that

$$\beta_i = \frac{-\theta_t \pm \alpha_i}{2}; \quad 1 \leq i \leq 2n + 1 \quad (39)$$

we can conclude that, throughout each minute, the solar tracking error assuming the Sun is fixed is less than 0.11° (so that the absorbed power on the Summer solstice decreases by less than 0.4%, actually much less, with respect to the optimal performance). However, if the solar tracking error reaches $\varepsilon = 0.36^\circ$ (something which happens if the tracking is updated only every 3 min), the power losses will start to be noticeable (possibly at least about 3%, just theoretically, without taking into account other causes).

Finally, we wish to stress the importance of having a suitable secondary reflective cavity. Consider the Summer solstice at noon (solar time). In Fig. 9 we show the same values as in Figs. 7 and 8, in the absence of secondary reflective cavity. For an error of 0.09° , the loss is essentially negligible (less than 1%). However, the power loss becomes significant (11%) for $\varepsilon = 0.18^\circ$ and totally unacceptable (32%) for $\varepsilon = 0.36^\circ$. This happens because, if there is no secondary reflective cavity, any reflected ray which does not fall on the absorber tube is, literally, lost.

As a consequence, an SSLFR without secondary cavity requires an extraordinarily precise tracking system. Otherwise, power losses might deem it completely ineffective.

In order to carry out the validation of our results, it would be necessary to have two identical (from the constructive point of view) prototypes of the SSLFR: one to be operated in the optimal conditions (errorless) and the other operated with solar tracking error, in order to obtain a good measure of the loss of absorbed energy. One could compute the thermal energy absorbed by the fluid and the thermal loss in the secondary reflector system, measuring the flow and temperature of the fluid at both ends of the tube. For its part, the thermal losses might be computed by interpolation, trying the secondary reflector system under different operational modes.

We think our contributions are useful for many possible future studies. An important aspect is to know the influence of wind on the SSLFR: wind would both affect the inclination of the primary mirrors and the position of the secondary reflector system, so that an optical error would appear, giving rise to losses in the absorbed energy.

7. Conclusions

This paper explores the effect on the absorbed power of possible solar tracking errors in the primary reflector system of a small-scale linear Fresnel reflector (SSLFR). The tracking of the motion of the Sun needs to be precise in order to prevent significant power losses. Using specifically developed Mathematica™ code, we provide an accurate assessment of the power absorbed by the absorber tube coming from each of the mirrors of an SSLFR under solar tracking errors. We compare the power losses under solar tracking error with the theoretical power production in optimal conditions.

Our main findings are that solar tracking errors have a highly non-linear direct influence on the ratio of loss of absorbed power: the larger the error, the (much) larger the loss ratio, so that very small solar tracking errors are acceptable, but they start being noticeable rather soon.

Regarding the influence of the mirrors, the power loss ratio is greater for the mirrors near the borders of the SSLFR. However (and this is remarkable), the total power loss ratio is, in general, similar to the power loss ratio for the central mirror; this is because extremal mirrors contribute less to the absorbed power. Also, because in our setting, the solar tracking error is the same for all mirrors, the power loss graph is not symmetrical with respect to the central mirror.

Moreover, the maximum and minimum power loss ratios need not take place either at the central mirror or at the borders: it depends greatly on the day and the solar time.

Finally, an SSLFR without secondary reflective cavity requires a very precise solar tracking system: errors which might be affordable under the presence of the secondary cavity become totally unacceptable without it.

We have developed a theoretical machinery which allows us to quantify the influence of “unavoidable” errors on the generated power (transmission errors, solar tracking errors ...); we have also developed the technique which allows us to optimize the motion of the mirrors in order to minimize the influence of the solar tracking error.

CRediT authorship contribution statement

A. Barbón: Conceptualization, Methodology. **C. Bayón-Cueli:** Methodology, Data curation. **L. Bayón:** Software, Methodology. **P. Fortuny Ayuso:** Software, Methodology, Writing - original draft.

Declaration of competing interest

The authors declare that they have no known competing financial interests or personal relationships that could have appeared to influence the work reported in this paper.

Acknowledgments

We wish to thank Dr. Laudino Rodríguez, head of the CIFP-Mantenimiento y Servicios a la Producción vocational training school in La Felguera, Asturias, Spain, for their work on the building of the prototype for the design presented in this paper.

References

- [1] BP Statistical Review of World Energy, 69th edition, 2020. Available at: <https://www.bp.com/>.
- [2] EUROSTAT. Database, Energy statistics-An overview, Available at: <https://ec.europa.eu/eurostat/statistics-explained/>, 2016.
- [3] European Commission, Energy-Heating and cooling, from, Available at: <https://ec.europa.eu/energy/en/topics/energyefficiency>. (Accessed 2 December 2019).
- [4] T. Schmidt, D. Mangold, H. Müller-Steinhagen, Central solar heating plants with seasonal storage in Germany, *Sol. Energy* 76 (2004) 165–174.
- [5] Euroheat & Power, Available from: <https://www.euroheat.org/news/record-breaking-solar-heating-system-ready-time/>. (Accessed 25 November 2019).
- [6] SDH, Solar District Heating Ranking list of European large-scale solar heating plants, Available from: <https://www.solar-district-heating.eu>. (Accessed 25 November 2019).
- [7] GStEC. Global, Solar thermal energy council, Available from: <https://www.solarthermalworld.org/installation/>. (Accessed 25 November 2019).
- [8] ARCON. Arcon, Solar, references. Arcon company website, Available from: <http://www.arcon.dk>. (Accessed 25 November 2019).
- [9] Y. Hang, M. Qu, F. Zhao, Economic and environmental life cycle analysis of solar hot water systems in the United States, *Energy Build.* 45 (2012) 181–188.
- [10] B. El Ghazzani, D. Martinez Plaza, R. Ait El Cadi, A. Ihlal, B. Abnay, K. Bouabid,

- Thermal plant based on parabolic trough collectors for industrial process heat generation in Morocco, *Renew. Energy* 113 (2017) 1261–1275.
- [11] G. Mokhtar, B. Boussad, S. Noureddine, A linear Fresnel reflector as a solar system for heating water: theoretical and experimental study, *Case Studies in Thermal Engineering* Case 8 (2016) 176–186.
- [12] N. El Gharbia, H. Derbalb, S. Bouaichaoua, N. Said, A comparative study between parabolic trough collector and linear Fresnel reflector technologies, *Energy Proced.* 6 (2011) 565–572.
- [13] A. Barbón, C. Bayón-Cueli, L. Bayón, L. Rodríguez, Investigating the influence of longitudinal tilt angles on the performance of small scale linear Fresnel reflectors for urban applications, *Renew. Energy* 143 (2019) 1581–1593.
- [14] M. Hack, G. Zhu, T. Wendelin, Evaluation and comparison of an adaptive method technique for improved performance of linear Fresnel secondary designs, *Appl. Energy* 208 (2017) 1441–1451.
- [15] M. El Ydrissi, H. Ghennoui, E. Ghali Bennouna, A. Farid, A review of optical errors and available applications of deflectometry technique in solar thermal power applications, *Renew. Sustain. Energy Rev.* 116 (2019) 109438.
- [16] A. Barbón, N. Barbón, L. Bayón, J.A. Otero, Theoretical elements for the design of a small-scale linear fresnel reflector: Frontal and lateral views, *Sol. Energy* 132 (2016) 188–202.
- [17] J.A. Duffie, W.A. Beckman, *Solar Engineering of Thermal Processes*, fourth ed., John Wiley & Sons, New York, 2013.
- [18] R. Oommen, S. Jayaraman, Development and performance analysis of compound parabolic solar concentrators with reduced gap losses—oversized reflector, *Energy Convers. Manag.* 42 (2001) 1379–1399.
- [19] R. Grena, P. Tarquini, Solar linear fresnel collector using molten nitrates as heat transfer fluid, *Energy* 36 (2011) 1048–1056.
- [20] S. Balaji, K.S. Reddy, T. Sundararajan, Optical modelling and performance analysis of a solar LFR receiver system with parabolic and involute secondary reflectors, *Appl. Energy* 179 (2016) 1138–1151.
- [21] Y. Qiu, M.-J. Li, K. Wang, Z.-B. Liu, X.-D. Xue, Aiming strategy optimization for uniform flux distribution in the receiver of a linear Fresnel solar reflector using a multi-objective genetic algorithm, *Appl. Energy* 205 (2017) 1394–1407.
- [22] J. Zheng, J. Yan, J. Pei, G. Liu, *Solar Tracking Error Analysis of Fresnel Reflector*, Hindawi Publishing Corporation The Scientific World Journal, 2014, p. 6. Article ID 834392.
- [23] I. Reda, A. Andreas, Solar position algorithm for solar radiation applications, *Sol. Energy* 76 (2004) 577–589.
- [24] J.J. Michalsky, The astronomical Almanac's algorithm for approximate solar position (1950–2050), *Sol. Energy* 40 (1988) 227–235.
- [25] M. Blanco-Muriel, D.C. Alarcon-Padilla, T. Lopea-Moratalla, M. Lara-Coira, Computing the solar vector, *Sol. Energy* 70 (2001) 431–441.
- [26] R. Grena, An algorithm for the computation of the solar position, *Sol. Energy* 82 (2008) 462–470.
- [27] G. Zhu, Development of an analytical optical method for linear Fresnel collectors, *Sol. Energy* 94 (2013) 240–252.
- [28] R. Grena, Five new algorithms for the computation of sun position from 2010 to 2110, *Sol. Energy* 86 (5) (2012) 1323–1337.
- [29] A. Barbón, J.A. Sánchez-Rodríguez, L. Bayón, C. Bayón-Cueli, Cost estimation relationships of a small scale linear Fresnel reflector, *Renew. Energy* 134 (2019) 1273–1284.
- [30] D.N. Korres, C. Tzivanidis, Development of two new semi-empirical formulas for estimation of solar absorptance in circular cavity receiver, *Therm. Sci. Eng. Prog.* 10 (2019) 147–153.
- [31] IDAE, Technical conditions for PV installations connected to the grid [in Spanish]. Spanish government technical Report. Report available from the publication services of the institute for diversification and energy savings, Spain, Available from: <http://www.idae.es>, 2011. (Accessed 10 January 2020).
- [32] A. Barbón, N. Barbón, L. Bayón, J.A. Otero, Optimization of the length and position of the absorber tube in small-scale Linear Fresnel Concentrators, *Renew. Energy* 99 (2016) 986–995.
- [33] G. Morin, J. Dersch, W. Platzer, M. Eck, A. Häberle, Comparison of linear Fresnel and parabolic trough collector power plants, *Sol. Energy* 86 (2012) 1–12.
- [34] G. Cau, D. Cocco, Comparison of medium-size concentrating solar power plants based on parabolic trough and linear Fresnel collectors, *Energy Procedia* 45 (2014) 101–110, 0.
- [35] Y. Elmaanaoui, D. Saifaoui, Parametric analysis of end loss efficiency in linear Fresnel reflector, in: *International Renewable and Sustainable Energy Conference, IRSEC IEEE*, 2014, pp. 104–107.
- [36] J.D. Nixon, P.A. Davies, Cost-exergy optimisation of linear Fresnel reflectors, *Sol. Energy* 86 (1) (2012) 147–156.
- [37] T. Sultana, G.L. Morrison, R. Taylor, G. Rosengarten, Performance of a linear fresnel rooftop mounted concentrating solar collector. 50th Australian Solar Energy Society Annual Conference, AuSE), Melbourne, Australia, 2012, pp. 6–7.
- [38] A. Heimsath, G. Bern, D. Van Rooyen, P. Nitz, Quantifying optical loss factors of small linear concentrating collectors for process heat application, *Energy Procedia* 48 (2014) 77–86.
- [39] A. Hofer, et al., Comparison of two different (quasi-) dynamic testing methods for the performance evaluation of a linear Fresnel process heat collector, *Energy Procedia* 69 (2015) 84–95.
- [40] P.L. Singh, R.M. Sarviya, J.L. Bhagoria, Thermal performance of linear Fresnel reflecting solar concentrator with trapezoidal cavity absorbers, *Appl. Energy* 87 (2) (2010) 541–550.
- [41] A. Barbón, N. Barbón, L. Bayón, J.A. Sánchez-Rodríguez, Parametric study of the small-scale linear Fresnel reflector, *Renew. Energy* 116 (2018) 64–74.
- [42] PVGIS. Joint research Centre (JRC), Available on line at, 2020., http://re.jrc.ec.europa.eu/pvg_tools/en/tools.html#PVP.
- [43] A. Barbón, P. Fortuny Ayuso, L. Bayón, J.A. Fernández-Rubiera, Predicting beam and diffuse horizontal irradiance using Fourier expansions, *Renew. Energy* 154 (2020) 46–57.
- [44] M. Binotti, G. Manzolini, G. Zhu, An alternative methodology to treat solar radiation data for the optical efficiency estimate of different types of collectors, *Sol. Energy* 110 (2014) 807–817.
- [45] M.A. Moghimi, K.J. Craig, J.P. Meyer, A novel computational approach to combine the optical and thermal modelling of Linear Fresnel Collectors using the finite volume method, *Sol. Energy* 116 (2015) 407–427.
- [46] A. Barbón, N. Barbón, L. Bayón, J.A. Sánchez-Rodríguez, Optimization of the distribution of small scale linear Fresnel reflectors on roofs of urban buildings, *Appl. Math. Model.* 59 (2018) 233–250.
- [47] M. Cagnoli, D. Mazzei, M. Procopio, V. Russo, L. Savoldi, R. Zanino, Analysis of the performance of linear Fresnel collectors: Encapsulated vs. evacuated tubes, *Sol. Energy* 164 (2018) 119–138.
- [48] V.M. Sharma, J.K. Nayak, S.B. Kedare, Effects of shading and blocking in linear Fresnel reflector field, *Sol. Energy* 113 (2015) 114–138.
- [49] P.H. Theunissen, W.A. Beckman, Solar transmittance characteristics of evacuated tubular collectors with diffuse back reflectors, *Sol. Energy* 35 (1985) 311–320.
- [50] H. Zheng, C. Feng, Y. Su, J. Dai, X. Ma, Design and experimental analysis of a cylindrical compound Fresnel solar concentrator, *Sol. Energy* 107 (2014) 26–37.